BIOCHEMISTRY
including biophysical chemistry & molecular biology

Article

pubs.acs.org/biochemistry

Long-Range Interaction between the Mn_4CaO_5 Cluster and the Non-heme Iron Center in Photosystem II as Revealed by FTIR Spectroelectrochemistry

Yuki Kato* and Takumi Noguchi*

Division of Material Science, Graduate School of Science, Nagoya University, Furo-cho, Chikusa-ku, Nagoya 464-8602, Japan

Supporting Information

ABSTRACT: It is known that inactivation of the Mn_4CaO_5 cluster, the catalytic center of water oxidation in photosystem II (PSII), induces a positive shift of the redox potential (E_m) of the primary quinone electron acceptor Q_A by ~+150 mV, resulting in suppression of the electron transfer from Q_A to the secondary quinone acceptor Q_B. Although the relevance of this $E_m(Q_A^-/Q_A)$ shift to the photoprotection of PSII has been debated, its molecular mechanism is still enigmatic from a structural viewpoint because Q_A is ~40 Å from the Mn_4CaO_5 cluster. In this work, we have investigated the influence of Mn depletion on the E_m of the non-heme iron, which is located between Q_A and Q_B, and its surrounding structure. Electrochemical measurements in combination with Fourier transform infrared (FTIR) spectroscopy revealed that Mn depletion shifts $E_m(Fe^{2+}/Fe^{3+})$ by +18 mV, which is ~8 times smaller than the shift of $E_m(Q_A^-/Q_A)$. Comparison of the Fe^{2+}/Fe^{3+} FTIR difference spectra between intact and Mn-depleted PSII samples showed that Mn depletion altered the pK_a's of a His ligand to the non-heme iron, most probably the D1-His215 interacting Q_B, and a carboxylate group, possibly D1-Glu244, coupled with the non-heme iron. It was further shown that Mn depletion influences the C≡N vibration of bromoxynil bound to the Q_B site, indicative of the modification of the Q_B binding site. On the basis of these results, we discuss the mechanism of a long-range interaction between the donor and acceptor sides of PSII.

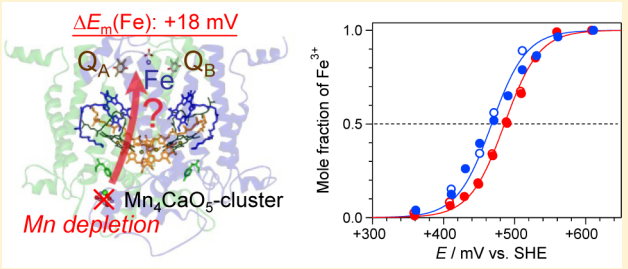

Photosystem II (PSII) is one of two photoactive protein complexes embedded in the thylakoid membranes of oxygenic photosynthetic organisms. Illumination of PSII forms a radical ion pair of the primary electron donor P680 and the acceptor pheophytin *a* (Phe *a*), which induces transmembrane electron transfer from the Mn_4CaO_5 cluster to plastoquinone (PQ).[1−4] The Mn_4CaO_5 cluster is the catalytic site of water oxidation, in which the reaction proceeds through stepwise oxidation of the S_n states, where n varies from 0 to 4.[5] The Mn_4CaO_5 cluster is oxidized by $P680^{+\bullet}$ via a redox-active tyrosine called Y_Z. On the electron-acceptor side, an electron from Phe $a^{-\bullet}$ is transferred to the primary quinone electron acceptor Q_A and then to the secondary quinone acceptor Q_B. Although Q_A exhibits only a one-electron reaction to relay an electron from Phe $a^{-\bullet}$ to Q_B, Q_B can accept two electrons to become plastoquinole (PQH_2) by taking up two protons.

Despite their identical chemical composition (PQ-9), for efficient electron transfer from Q_A to Q_B the gap of their redox potentials should be elaborately tuned by interactions with the surrounding proteins. The redox potential of Q_A, $E_m(Q_A^-/Q_A)$, in intact PSII preparations has been reported to be around −100 mV,[6−12] whereas $E_m(Q_B^-/Q_B)$ has been estimated to be higher than $E_m(Q_A^-/Q_A)$ by about 80 mV.[13−15] It is known, however, that the $E_m(Q_A^-/Q_A)$ value is significantly altered by the perturbation of PSII. It was demonstrated that the removal of the Mn and/or Ca ions from PSII, resulting in the inhibition of water oxidation, shifts $E_m(Q_A^-/Q_A)$ by about +150 mV.[6−12] As a consequence of this $E_m(Q_A^-/Q_A)$ shift, the forward electron transfer from Q_A to Q_B is suppressed, as was shown by fluorescence kinetics measurements.[16] In contrast, on photoassembly of the Mn_4CaO_5 cluster, $E_m(Q_A^-/Q_A)$ was found to shift back to a lower potential by about 150 mV,[8] which was also verified by fluorescence kinetics measurements.[17] Physiologically, these phenomena are explained with relevance to photoprotection:[3,8,18,19] the positive shift of $E_m(Q_A^-/Q_A)$ results in the increase in the E_m gap between Q_A and Phe *a* and hence direct charge recombination between Q_A^- and $P680^{+\bullet}$ is promoted rather than indirect recombination via $P680^{+\bullet}$ Phe $a^{-\bullet}$, which leads to the formation of harmful singlet oxygen via a chlorophyll triplet state. In relation to the effect of Ca^{2+} depletion, Ca^{2+}/Sr^{2+} exchange was also found to shift $E_m(Q_A^-/Q_A)$ by +27 mV,[20] which is less than the effect of Ca^{2+} depletion, presumably leading to deceleration of the Q_A to Q_B electron transfer in Ca^{2+}/Sr^{2+}-exchanged PSII complexes.[21]

Besides perturbation on the donor side, it has been reported that $E_m(Q_A^-/Q_A)$ is influenced by herbicide binding to the Q_B site:[22] bromoxynil, a phenol-type herbicide, shifts $E_m(Q_A^-/Q_A)$ in a negative direction by ~45 mV, whereas a positive shift of

Received: May 9, 2014
Revised: July 15, 2014
Published: July 16, 2014

~50 mV is induced by a urea-type herbicide, 3-(3,4-dichlorophyenyl)-1,1-dimethylurea (DCMU). The herbicide-induced $E_m(Q_A^-/Q_A)$ shifts alter the charge recombination pathways and thus affect the sensitivity to photodamage.[23,24] Q_A and Q_B are symmetrically located around the non-heme iron,[25−27] which exists at the interface of the two major proteins, the D1 and D2 subunits, as shown in the X-ray crystallographic structures of PSII complexes[28−31] (Figure 1).

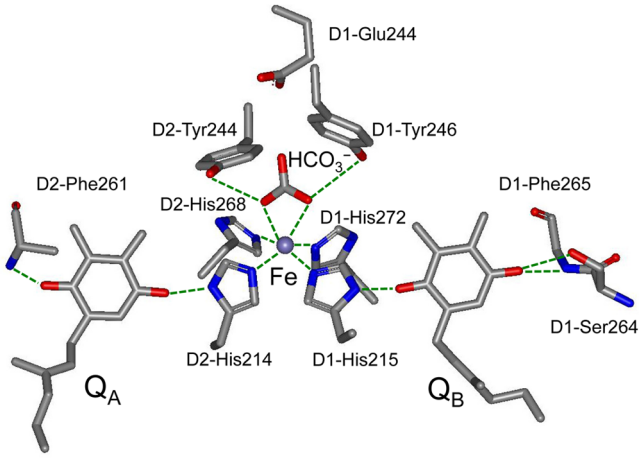

Figure 1. Structure around the non-heme iron center deduced from the X-ray crystallographic structure of PSII at 1.9 Å resolution (PDB code: 3ARC[31]).

Q_A and Q_B are linked to each other through a molecular bridge, Q_A-His214(D2)-Fe-His215(D1)-Q_B, formed with two His ligands to the non-heme iron. The molecular mechanism of the $E_m(Q_A^-/Q_A)$ shifts by herbicide binding has been examined by Fourier transform infrared (FTIR) difference spectroscopy and theoretical calculations.[32,33] Different directions of the shifts in the CO stretching frequency of Q_A^- were detected on binding of different types of herbicides in light-induced FTIR difference spectra,[32] and it was suggested that the hydrogen-bond interaction between D1-His215 and the herbicide at the Q_B site influences the hydrogen-bond strength between D2-His214 and the Q_A C═O through this molecular bridge, resulting in the shift of $E_m(Q_A/Q_A^-)$.[32,33]

In contrast, the molecular mechanism of the $E_m(Q_A^-/Q_A)$ shifts induced by the perturbation of the Mn_4CaO_5 cluster remains unclear.[3] Such a long-range interaction across the membrane (the distance between the Mn_4CaO_5 cluster and Q_A is about 40 Å) seems difficult to accept. A likely hypothesis is that the membrane spanning helices mediate the structural changes.[6] However, the Mn_4CaO_5 cluster mainly interacts with the D1 subunit, whereas the Q_A site is formed with the D2 subunit. It is thus possible that the perturbation of the Mn_4CaO_5 cluster is transferred to the Q_B site first through the transmembrane helices of the D1 subunit and then to the Q_A site by the molecular bridge involving the non-heme iron. If this were the case, then the redox properties not only of Q_A but also of the non-heme iron and Q_B would be influenced by the perturbation of the Mn_4CaO_5 cluster.[3] However, such a donor-side effect on the non-heme iron center and the Q_B site has not been reported to date except for an EPR study in which the non-heme iron environment was slightly modified by Ca/Sr exchange.[34]

In this study, we have investigated the influence of Mn depletion on the redox potential of the non-heme iron, $E_m(Fe^{2+}/Fe^{3+})$, and its surrounding structure involving the Q_B site to shed new light on the mechanism of the long-range interaction in PSII. For this purpose, we have used an electrochemical method in combination with light-induced FTIR difference spectroscopy. Spectroelectrochemistry using thin-layer cells has been used to measure the E_m of various redox cofactors in photosystems within an error range of a few millivolts,[9,10,20,35−37] which is often smaller than that by chemical titration. Meanwhile, light-induced FTIR difference spectroscopy is a powerful method for studying the structures and interactions of redox cofactors and surrounding moieties.[38−43] Thus, the combination of FTIR spectroscopy with electrochemistry would be more fruitful for investigating the relationship between the redox properties of cofactors and the structures of the binding sites.

The non-heme iron has an $E_m(Fe^{2+}/Fe^{3+})$ value around +400 mV (pH 7.0)[27,44−48] and hence is readily oxidized by an oxidant such as ferricyanide. This preoxidized Fe^{3+} functions as an endogenous electron acceptor, and it is reduced to Fe^{2+} by illumination. Utilizing this redox property of the non-heme iron, its FTIR spectrum has been obtained as a light-induced Fe^{2+}-minus-Fe^{3+} (hereafter expressed as Fe^{2+}/Fe^{3+}) difference spectrum,[33,37,48−52] providing structural information on the protein moieties around the non-heme iron and also on the Q_B binding site. Here, we have controlled the redox reaction of the non-heme iron by an electrochemical method and then measured light-induced Fe^{2+}/Fe^{3+} FTIR difference spectra using both intact and Mn-depleted PSII preparations. In this way, the influence of Mn depletion on $E_m(Fe^{2+}/Fe^{3+})$ together with that of the surrounding structure was examined. With the obtained results, the mechanism of the long-range interaction between the donor and acceptor sides of PSII is discussed.

MATERIALS AND METHODS

Oxygen-evolving PSII-enriched membranes were prepared from spinach following a method that was previously described[53] and suspended in a MES buffer containing 40 mM MES-NaOH (pH 6.5), 400 mM sucrose, and 15 mM NaCl. The oxygen-evolving activity of the obtained PSII samples was about 500 μmol of O_2 mg Chl^{-1} h^{-1}. Mn depletion was performed by incubating the PSII membranes in MES buffer additionally containing 10 mM NH_2OH and 0.5 mM EDTA·2Na at 0 °C for 20 min in the dark. The NH_2OH-treated PSII membranes were subsequently washed with the former MES buffer three times. Before measurements, both the intact and Mn-depleted samples were suspended at a concentration of 0.5 mg of Chl mL^{-1} in an electrolytic solution containing 40 mM MES-NaOH (pH 6.5), 400 mM sucrose, 15 mM NaCl, 5 mM $CaCl_2$, 40 mM $NaHCO_3$, 200 mM KCl, and the following redox mediators: 100 μM $Ru(NH_3)_6Cl_2$ (E_m = +51 mV), 100 μM ferrocenylmethyl trimethylammonium (E_m = +627 mV), and a redox couple of 10 mM $K_4Fe(CN)_6$ and 10 mM $K_3Fe(CN)_6$ (E_m = +430 mV). The total concentration of the $K_4Fe(CN)_6/K_3Fe(CN)_6$ couple was the same as in a previous report,[48] and this redox couple works not only as a redox mediator but also as an exogenous electron donor/acceptor during the light reaction in PSII. For measurement of a standard S_2/S_1 difference spectrum without contributions of the signals from the acceptor side, a 100 mM MES-NaOH (pH 5.5) buffer containing the same concentrations of salts, sucrose, and redox mediators was used. The buffer was used at pH 5.5 instead of pH 6.5[48,54] because a lower pH value shifts $E_m(Fe^{2+}/Fe^{3+})$ positively due to its pH dependence (−60 mV/

dx.doi.org/10.1021/bi500549b | Biochemistry 2014, 53, 4914−4923

pH[27,45,47,48]) and thus prevents preoxidation of the non-heme iron even at a relatively high potential (+430 mV), which was used to promote abstraction of an electron from Q_A. When necessary, bromoxynil (5 μM) was involved in the electrolytic solution. The sample in the electrolytic solution was centrifuged at 170 000*g* for 35 min, and the resulting pellet was transferred to a spectroelectrochemical cell for FTIR measurements. For deuteration of intact PSII membranes, the PSII samples were suspended with D_2O solution (40 mM MES-NaOD, pD 6.5 or 200 mM MES-NaOD, pD 5.5) containing the same concentrations of salts, deuterated sucrose, and mediators as that used in the H_2O electrolytic solution, and then the centrifuged pellet was used for FTIR measurements.

An optically transparent thin-layer electrode (OTTLE) cell similar to the one previously reported[55,56] was used for FTIR spectroelectrochemical measurements. A gold mesh (60% transparent, 6 μm thick; Precision Eforming LLC.), which was chemically modified with a solution of 4,4′-dithiodipyridine[57] beforehand, served as the working electrode. The sample pellet was loaded on the gold mesh placed on a CaF_2 plate (25 mm diameter) in a cell body (internal diameter of 27 mm), and was sandwiched with another CaF_2 plate. The sample was then squeezed tightly, forming a sample layer of ~15 μm thickness. A Pt black wire as the counter electrode and a Ag/AgCl/3 M KCl reference electrode (2 mm diameter; Cypress Systems Inc., 66-EE009) were placed around the periphery of the CaF_2 plates.[56] For an electric contact between the gold working electrode and the other two electrodes, the space around the periphery of the CaF_2 plates was filled with the electrolytic solution (ca. 500 μL). It was confirmed by monitoring FTIR absorption that the sample between the CaF_2 plates was diluted with the surrounding solution by less than 5% even after 24 h.

Flash-induced FTIR spectra were recorded on a Bruker IFS-66/S spectrophotometer equipped with an MCT detector (D313-L/3) at 4 cm^{-1} resolution. The OTTLE cell was set in a copper holder, and the sample temperature was adjusted to 10 °C by circulating cold water in the holder. The electrode potential was controlled using a potentiostat (model 2020, Toho Technical Research). In this article, the electrode potential is hereafter expressed against the standard hydrogen electrode (SHE) (0 mV vs Ag/AgCl/3 M KCl is equivalent to +208 mV vs SHE). For each FTIR measurement, an accurate electrode potential of the Ag/AgCl/3 M KCl reference electrode was recorded using a standard Ag/AgCl/saturated KCl electrode (+199 mV vs SHE), and corrected electrode potentials were used for evaluating the redox potential of the non-heme iron. Flash illumination was performed using a Q-switched Nd:YAG laser (Quanta-Ray INDI-40-10; 532 nm, ~7 ns full width at half-maximum, ~7 mJ $pulse^{-1}$ cm^{-2}). For estimation of $E_m(Fe^{2+}/Fe^{3+})$, single-beam spectra with 50 scans (accumulation for 25 s) were recorded before and after single-flash illumination at a series of electrode potentials. At each electrode potential, the sample was incubated for 30 min to equilibrate the redox reaction. To obtain higher-quality spectra of the S_2/S_1, S_2Fe^{2+}/S_1Fe^{3+}, and Fe^{2+}/Fe^{3+} differences at certain electrode potentials, 20 scan measurements before and after flash illumination were repeated 24−36 times with a dark interval of 30 min. For the S_2/S_1 spectrum, an interval of 2 s was inserted after flash illumination to remove the contamination of Q_A signals.

RESULTS

Figure 2a−j shows FTIR difference spectra (1500−1050 cm^{-1} region) upon single-flash illumination of the intact PSII membranes in an electrolytic solution at pH 6.5 equilibrated at a series of electrode potentials between +350 and +600 mV (vs SHE). Flash illumination induces single-turnover electron transfer from the electron-donor side to the acceptor side. In intact PSII, the dark-stable S_1 state is converted to the S_2 state on the donor side, whereas on the acceptor side, the non-heme iron accepts an electron when it is preoxidized or otherwise an electron is abstracted by an exogenous electron acceptor, ferricyanide. Indeed, the difference spectra constantly showed signals at 1439, 1419, 1404, and 1365 cm^{-1}, which are virtually identical to the signals in standard S_2/S_1 difference spectra reported previously[48,54,58,59] and also obtained at +430 mV using the intact PSII membranes at pH 5.5 (Figure 2k). These bands in the 1450−1350 cm^{-1} region in the S_2/S_1 difference spectrum have been assigned to the symmetric stretching vibrations of carboxylate groups surrounding the Mn_4CaO_5 cluster.[54,58,59] The presence of these S_2/S_1 signals, in turn, confirms that the Mn_4CaO_5 cluster in the PSII sample remains intact during the measurements at a series of electrode potentials.

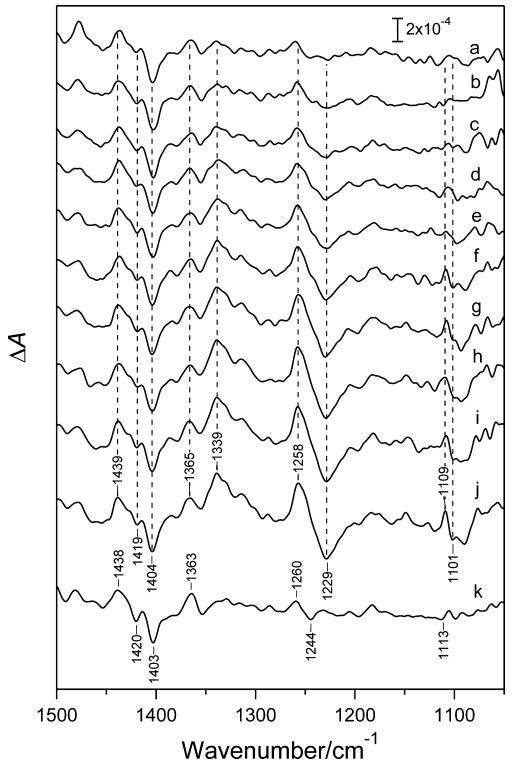

Figure 2. Flash-induced FTIR difference spectra representing an S_2Fe^{2+}/S_1Fe^{3+} difference (1500−1050 cm^{-1} region) of the intact PSII membranes at a series of electrode potentials: +350 mV (a), +400 mV (b), +420 mV (c), +440 mV (d), +460 mV (e), +480 mV (f), +500 mV (g), +520 mV (h), +550 mV (i), and +600 mV (j). A standard S_2/S_1 difference spectrum (k) is shown for comparison. The spectra in a−j were measured at pH 6.5. The spectrum in k was measured at +430 mV at pH 5.5, and spectra obtained using two different samples were averaged.

In contrast to the bands of the Mn_4CaO_5 cluster, bands at 1339, 1258, 1229, 1109, and 1101 cm^{-1} decreased in intensity at lower potentials (Figure 2a−j). These signals are virtually

dx.doi.org/10.1021/bi500549b | *Biochemistry* 2014, 53, 4914−4923

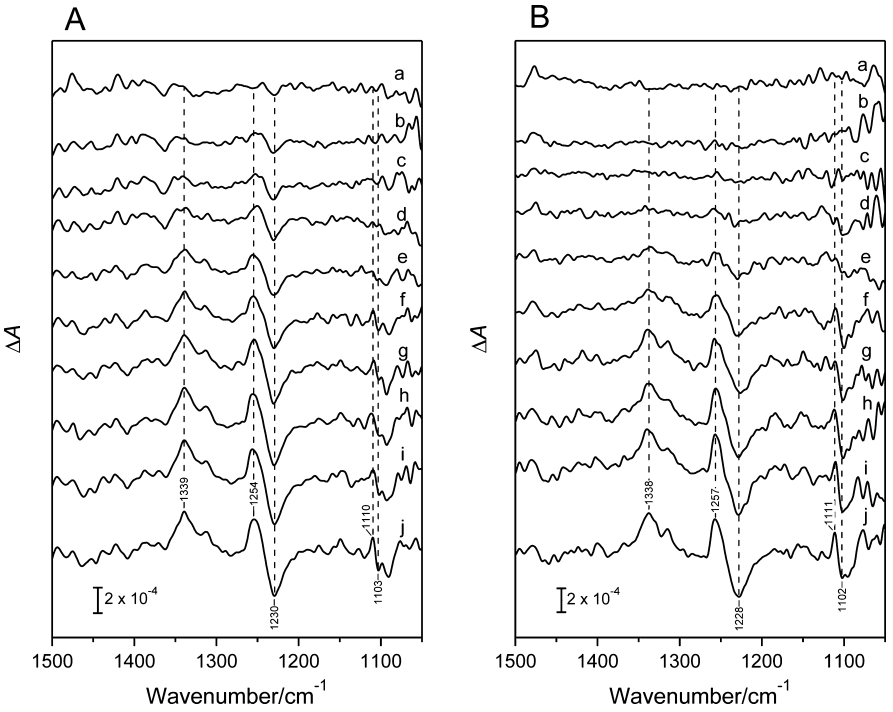

Figure 3. Fe^{2+}/Fe^{3+} FTIR difference spectra (1500−1050 cm^{-1} region) of the intact (A) and Mn-depleted PSII membranes (B) at a series of electrode potentials: +350 mV (a), +400 mV (b), +420 mV (c), +440 mV (d), +460 mV (e), +480 mV (f), +500 mV (g), +520 mV (h), +550 mV (i), and +600 mV (j). The Fe^{2+}/Fe^{3+} spectra in panel A were obtained by subtraction of the S_2/S_1 difference spectrum (Figure 2k) from the S_2Fe^{2+}/S_1Fe^{3+} difference spectra (Figure 2a−j).

identical to the ones in the Fe^{2+}/Fe^{3+} difference spectra of the non-heme iron previously obtained using spinach PSII membranes[33,48−50] and cyanobacterial PSII core complexes.[51,52] The positive and negative bands at 1339 and 1229 cm^{-1}, respectively, were assigned to the symmetric CO stretching vibrations of bicarbonate, a ligand of the non-heme iron, by [^{13}C]bicarbonate labeling,[49] whereas a major contribution of the positive band at 1258 cm^{-1} and a part of the negative 1229 cm^{-1} band were attributed to the CO stretching vibrations of a Tyr side chain (either D1-Tyr246 or D2-Tyr244) coupled to the non-heme iron by [4-^{13}C]Tyr labeling.[52] The peaks at 1109 and 1101 cm^{-1} were assigned to the CN stretching vibrations of the His ligands by ^{15}N labeling.[49] The larger intensities of these signals at a higher electrode potential indicate that a larger fraction of the non-heme iron centers is preoxidized to Fe^{3+} at a higher potential. Indeed, the CN bands of ferricyanide/ferrocyanide at 2116/2039 cm^{-1} were hardly detected at +550 mV and higher potentials (Figure S1, blue line in Supporting Information), indicating that an electron is trapped by the non-heme iron. The 1700−1500 cm^{-1} region of the obtained spectra (data not shown) involves mainly the amide I and II vibrations of backbone amides coupled to the S_1-to-S_2[54,58,59] and Fe^{3+}-to-Fe^{2+}[49−52] changes. We do not discuss the signals in this region in the present work because this region is mostly saturated (the original absorbance is more than 1.0) due to the large absorption bands of water and protein main chains; hence, the spectra suffer from high noise levels and baseline changes (Figure S1).

Although the prominent signals of the Mn_4CaO_5 cluster are rather separated from those of the non-heme iron, some minor peaks at 1260/1244 and 1113 cm^{-1} (Figure 2k) still superimpose the non-heme iron signals at 1258/1229 and 1109/1101 cm^{-1} (Figure 2a−j), respectively. Note that these minor peaks in the S_2/S_1 spectrum obtained in this study (Figure 2k) have also been observed in standard S_2/S_1 spectra reported previously.[48,54,58,59] Hence, for accurate estimation of the intensities of the non-heme iron signals, the S_2/S_1 difference spectrum (Figure 2k) was subtracted from the spectra in Figure 2a−j with appropriate factors to cancel the bands near 1400 cm^{-1} to remove the contribution of the S_2/S_1 signals. The obtained Fe^{2+}/Fe^{3+} difference spectra of intact PSII are shown in Figure 3A in comparison with the Fe^{2+}/Fe^{3+} difference spectra obtained using the Mn-depleted PSII membranes (Figure 3B). In the latter Mn-depleted sample, an electron hole is abstracted by ferrocyanide and hence only the signals of the non-heme iron on the electron=acceptor side are observed. Indeed, in all of these spectra, a negative peak at 2039 cm^{-1} due to the ferrocyanide CN vibration was observed (the spectrum at +550 mV is shown in Figure S1, red line in Supporting Information), implying the consumption of ferrocyanide on the electron-donor side. Comparison of the non-heme iron signals between the intact and Mn-depleted PSII samples shows that the shapes and frequencies of the major peaks in 1500−1000 cm^{-1} are mostly identical between the two samples.

The molar ratio of the two redox states of the non-heme iron at a series of electrode potentials was evaluated using the intensity difference of the two prominent bands at 1257−1254 and 1230−1228 cm^{-1}. The relationship between the Fe^{3+}/Fe^{2+} ratio and the electrode potential is shown in Figure 4 for the intact (blue symbols) and Mn-depleted (red symbols) PSII samples. The plots of the data in the oxidative (closed symbols) and reductive (open symbols) potential steps are mostly identical, indicative of a reversible reaction. The semi-logarithmic plots (Figure 4A) show a linear relationship, with

dx.doi.org/10.1021/bi500549b | *Biochemistry* 2014, 53, 4914−4923

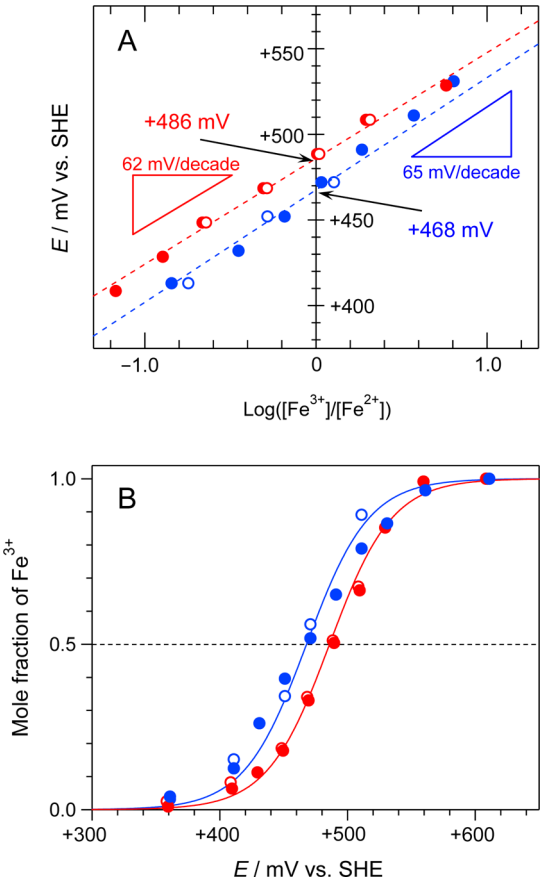

Figure 4. Nernstian plots of the redox reactions of the non-heme iron in the intact (blue symbols) and Mn-depleted PSII membranes (red symbols). The closed and open symbols indicate the data of oxidative and reductive potential steps, respectively. (A) Semilogarithmic plots, revealing regression lines (broken lines) with slopes of 65 mV decade^{-1} (intact) and 62 mV decade^{-1} (Mn-depleted) and intercepts as the E_m values of +468 mV (intact) and +486 mV (Mn-depleted). (B) Plots with theoretical Nernstian curves assuming one-electron redox processes with E_m = +468 (intact) and +486 mV (Mn-depleted).

slopes of 65 and 62 mV decade^{-1} for the intact and Mn-depleted PSII, respectively. Although these slopes are somewhat higher than the theoretical value of 56 mV at 10 °C (the measurement temperature), the data from both PSII samples satisfactorily agree with the theoretical one-electron Nernstian curves (Figure 4B), confirming a one-electron redox reaction of the non-heme iron. Other prominent bands at 1339 and 1102 cm^{-1} also showed similar potential dependences (plots not shown).

The Nernstian analyses revealed $E_m(Fe^{2+}/Fe^{3+})$ values of +468 ± 3 and +486 ± 4 mV for the intact and Mn-depleted PSII membranes, respectively. These $E_m(Fe^{2+}/Fe^{3+})$ values obtained at pH 6.5 are more positive by 10−40 mV than the values of previous measurements using PSII membranes,[46−48] even when taking into consideration the pH dependence of $E_m(Fe^{2+}/Fe^{3+})$ (−60 mV/pH[27,45,47,48]). This difference could be related to the presence of a relatively high concentration of bicarbonate (40 mM) in the present samples, which was necessary to stabilize the structure and reaction of the non-heme iron, in contrast to the absence of additional bicarbonate in previous works.[46−48] Regardless of the absolute $E_m(Fe^{2+}/Fe^{3+})$ values, the results of the present FTIR spectroelectrochemistry study demonstrate that Mn depletion shifts the $E_m(Fe^{2+}/Fe^{3+})$ value positively by 18 mV. This value is about 8 times smaller than the shift of $E_m(Q_A^-/Q_A)$ (~+150 mV[6−12]) on Mn depletion.

To investigate the influence of Mn depletion on the structure around the non-heme iron, Fe^{2+}/Fe^{3+} difference spectra of the intact and Mn-depleted PSII samples at +550 mV in the electrolytic solution at pH 6.5 were compared in more detail (Figure 5). To improve the spectral quality, the S_2Fe^{2+}/S_1Fe^{3+}

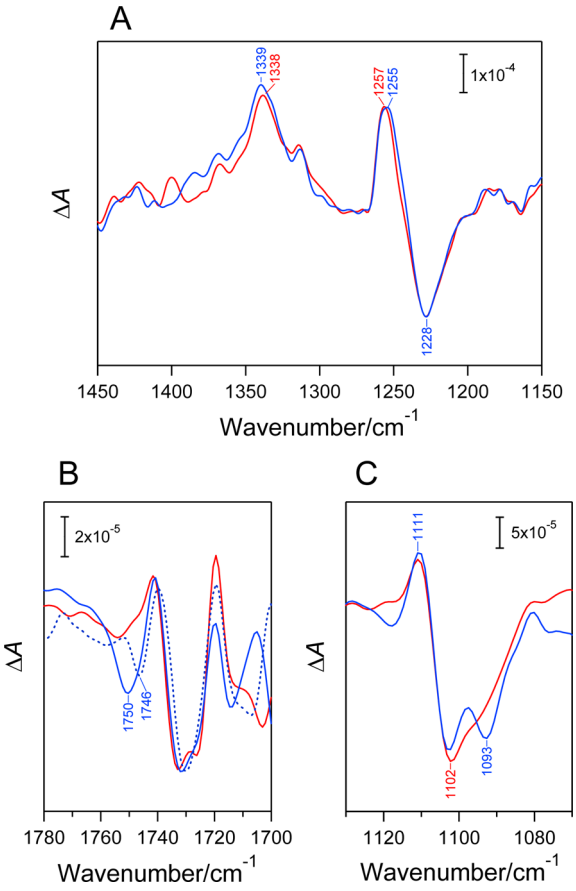

Figure 5. (A) Comparison of the Fe^{2+}/Fe^{3+}spectra of the intact (blue line) and Mn-depleted (red line) PSII membranes in the regions of the CO stretches of bicarbonate and Tyr (A; 1450−1150 cm^{-1}), the C═O stretch of COOH (B; 1780−1700 cm^{-1}), and the CN stretch of His (C; 1130−1070 cm^{-1}). The spectrum of intact PSII membranes was obtained by subtraction of the S_2/S_1 spectrum (Figure 2k) from the S_2Fe^{2+}/S_1Fe^{3+} spectrum (Figure S2a, black line). The corresponding Fe^{2+}/Fe^{3+} spectrum of intact PSII in D_2O buffer is also presented in panel B (blue dotted line). The S_2Fe^{2+}/S_1Fe^{3+} and Fe^{2+}/Fe^{3+} difference spectra of the intact and Mn-depleted PSII samples, respectively, were measured at +550 mV at pH(D) 6.5.

and Fe^{2+}/Fe^{3+} spectra of the intact and Mn-depleted PSII membranes, respectively, were measured repeatedly more than 20 times for each sample, and the spectra using two different samples were averaged. The Fe^{2+}/Fe^{3+} difference spectrum of the intact PSII was obtained by subtraction of the S_2/S_1 spectrum (Figure 2k) from the thus obtained S_2Fe^{2+}/S_1Fe^{3+} spectrum (Figure S2 in Supporting Information). The shapes and the frequencies of the bicarbonate CO bands at 1339 and 1228 cm^{-1} were virtually unchanged on Mn depletion, whereas a slight upshift by 2 cm^{-1} was detected in the Tyr CO band at 1255 cm^{-1} (Figure 5A), indicating that the interaction of the coupled Tyr side chain (either D1-Tyr246 or D2-Tyr244) is

dx.doi.org/10.1021/bi500549b | Biochemistry 2014, 53, 4914−4923

slightly affected by Mn depletion. A clearer change was detected in the feature of the His CN stretching band near 1100 cm^{-1} (Figure 5C). In intact PSII, the negative band splits into 1102 and 1093 cm^{-1}, and the relative intensity of the latter peak decreased on Mn depletion. The 1093 cm^{-1} signal was previously attributed to deprotonation of one of the four His ligands, most probably D1-His215 in the Q_B binding site, to become the imidazolate form in the Fe^{3+} state.[49,50] It has also been shown that the appearance of this peak is sensitive to herbicide binding at the Q_B site,[33,50] strongly supporting the assignment of the 1093 cm^{-1} peak to D1-His215. If this assignment is correct, then the intensity decrease of the 1093 cm^{-1} band on Mn depletion (Figure 5C) would indicate that the pK_a of D1-His215 in the Fe^{3+} state is increased by this treatment.

Another change was observed in the C═O stretching region of protonated carboxylic acid[60,61] at 1760−1700 cm^{-1} (Figure 5B). This region generally shows only the COOH vibrations in proteins, although the ester C═O vibrations of chlorophyll and pheophytin could overlap in this region.[62] The latter vibration, however, often appears as a differential signal due to an electrochromic shift or some change in the interaction with the protein. In this COOH region, it was clearly seen that the negative band at 1750 cm^{-1} in intact PSII disappeared in Mn-depleted PSII. Similar measurements of intact PSII in D_2O showed that this band at 1750 cm^{-1} downshifted by 4 cm^{-1} upon deuteration (Figure 5B, blue dotted line), confirming the assignment to a COOH vibration. These observations indicate that in intact PSII a COOH group near the non-heme iron is deprotonated upon photoreduction of Fe^{3+}, whereas in Mn-depleted PSII, the protonation structure of this carboxylate group is unchanged by this reaction. Peaks at 1741, 1732, and 1719 cm^{-1} were virtually unchanged by deuteration of intact PSII and hence are probably attributable to the electrochomic shifts of the ester C═O groups of chlorophyll or pheophytin. The spectral features at 1710−1700 cm^{-1}, which were sensitive to deutertion, were altered by Mn depletion (Figure 5B), suggesting the possibility that protonation/deprotonation reactions of some other carboxylic groups near the non-heme iron could be affected by Mn depletion.

Fe^{2+}/Fe^{3+} difference spectra of the intact and Mn-depleted PSII samples in the presence of bromoxynil, a phenolic herbicide, were measured to gain structural information on the Q_B binding site through the vibrational modes of bromoxynil. In particular, the C≡N stretching band of its nitrile group has been detected at 2220−2200 cm^{-1} without interference from other bands in the Fe^{2+}/Fe^{3+} difference spectra,[32,33,37] indicative of the structural coupling of bromoxynil in the Q_B site with the non-heme iron. Hence, we utilized this C≡N band as a probe of the structural change of the Q_B site. Figure 6 shows the Fe^{2+}/Fe^{3+} difference spectra of PSII in the presence of bromoxynil in the regions of its C≡N stretch (A; 2240−2180 cm^{-1}) and of the CO stretches of bicarbonate and Tyr and the His CN stretch (B; 1500−1050 cm^{-1}). The peaks in the latter region (Figure 6B) were virtually identical between the intact and Mn-depleted samples, although the band features were slightly different from those in the absence of bromoxynil (Figure 5A,C) as previously reported.[33] In particular, the feature of the His bands around 1100 cm^{-1} was unchanged even on Mn depletion, probably due to strong hydrogen bonding of the NH of D1-His215 to the phenolate CO of bromoxynil.[33] This unchanged hydrogen bonding is consistent with the observation that a positive peak at 1516 cm^{-1}, which

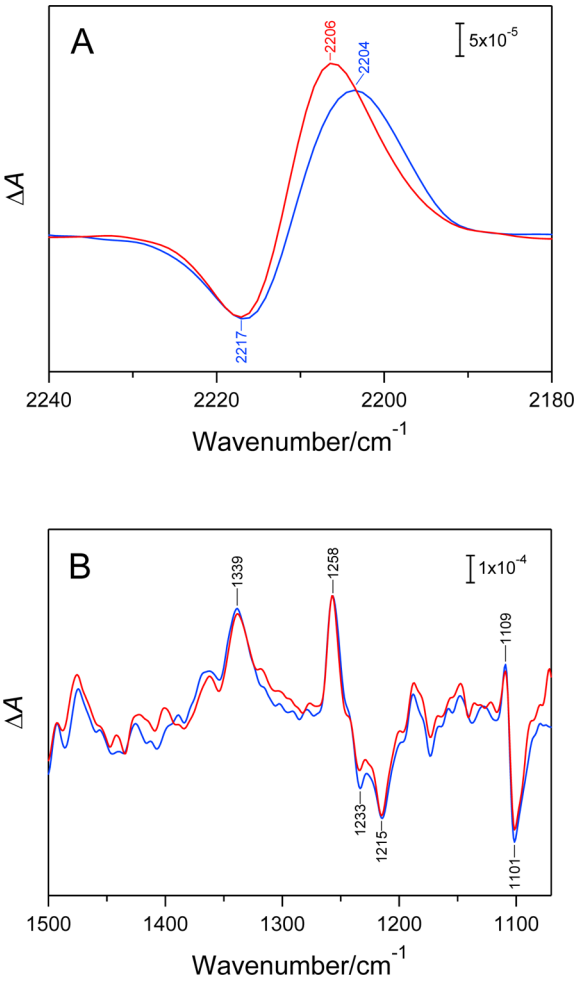

Figure 6. Fe^{2+}/Fe^{3+} difference spectra of the intact (blue line) and Mn-depleted (red line) PSII membranes in the presence of bromoxynil in its C≡N stretch region (A; 2240−2180 cm^{-1}) and in the region of the bicarbonate and Tyr CO and the His CN vibrations (B; 1500−1070 cm^{-1}). The spectrum of the intact PSII (blue line) was obtained by subtraction of the S_2/S_1 difference spectrum (Figure 2k) from the S_2Fe^{2+}/S_1Fe^{3+} difference spectrum in the presence of bromoxynil. The spectra were measured at 550 mV at pH 6.5.

was previously attributed to the CO stretching vibration of the phenolate group of deprotonated bromoxynil,[33] was not affected by Mn depletion (data not shown). In contrast, the C≡N signal of bromoxynil was affected by Mn depletion (Figure 6A). The positive band at 2204 cm^{-1} was clearly upshifted by 2 cm^{-1} with a narrower width on Mn depletion (Figure 6A), whereas the negative peak at 2217 cm^{-1} was virtually unchanged. This observation indicates that the hydrogen-bond interaction of the C≡N group of bromoxynil to the protein was weakened due to some modification of the Q_B site by Mn depletion when the non-heme iron is in the reduced Fe^{2+} state.

DISCUSSION

The non-heme iron is a redox-active cofactor located between Q_A and Q_B in PSII, showing E_m values around +400 mV at pH 7.0 with a pH dependence of −60 mV/pH unit.[25−27,44−48] In spite of its redox activity, the non-heme iron does not directly participate in the electron transfer from Q_A to Q_B because of its much higher $E_m(Fe^{2+}/Fe^{3+})$ value compared with those of Q_A

dx.doi.org/10.1021/bi500549b | Biochemistry 2014, 53, 4914−4923

and Q_B.[4,25,63] However, the pH dependence of $E_m(Fe^{2+}/Fe^{3+})$ implies that its redox reaction is coupled to a nearby protonatable residue(s) in the hydrogen-bond network, which may be involved in the proton pathway to Q_B.[46,50,64,65] Here, we focused on the effect of Mn depletion on the redox property and the structure of the non-heme iron center to study the long-range interaction between the electron-donor and -acceptor sides of PSII. In particular, we have directly detected the structural changes of the protein moieties around the non-heme iron on Mn depletion by measuring light-induced FTIR difference spectra at controlled electrode potentials.

The FTIR spectroelectrochemical measurements revealed that Mn depletion of PSII preparation induces a positive shift of $E_m(Fe^{2+}/Fe^{3+})$ by 18 mV (Figure 4). This non-negligible $E_m(Fe^{2+}/Fe^{3+})$ shift should be caused by the structural changes near the non-heme iron upon Mn depletion. Indeed, comparison of the Fe^{2+}/Fe^{3+} difference spectra between the intact and Mn-depleted PSII samples (Figure 5) exhibited small but clear differences in the His CN and COOH regions. In the CN stretching region of His around 1100 cm^{-1}, which provides information on the protonation structure of His,[66] there are two negative peaks at 1102 and 1093 cm^{-1} in intact PSII at pH 6.5, whereas the latter peak diminished on Mn depletion (Figure 5C). The peak at 1093 cm^{-1} has been attributed to the deprotonated anion form of a His ligand, most probably D1-His215 interacting Q_B.[33,49,50] Thus, the N_π-H of D1-His215 would be deprotonated in intact PSII when the non-heme iron is in the oxidized Fe^{3+} state. The intensity decrease of this peak in Mn-depleted PSII (Figure 5C) indicates that the pK_a of D1-His215 increased, and this His was protonated to the neutral $N_\pi H$ form on Mn depletion.

A clear negative band at 1750 cm^{-1} in the C=O stretching region of COOH in the Fe^{2+}/Fe^{3+} spectrum (Figure 5B) reflects deprotonation of a COOH group on reduction of Fe^{3+} in intact PSII, whereas this reaction was not detected in Mn-depleted PSII. This COOH group coupled to the non-heme iron may originate from one of the several Glu residues (D1-Glu226, D1-Glu242, D1-Glu243, D1-Glu244, D2-Glu241, and D2-Glu242) located on the stromal side of the non-heme iron. The best candidate is D1-Glu244, which is coupled to the non-heme iron through bicarbonate. Indeed, previous calculations by Ishikita and Knapp[67] using the linearized Poisson–Boltzmann equation predicted the involvement of protonation/deprotonation of this Glu residue for the pH dependence of $E_m(Fe^{2+}/Fe^{3+})$. The previous Fe^{2+}/Fe^{3+} difference spectrum measured using Mn-deleted PSII membranes of spinach at pH 8.0 exhibited a similar negative band at 1752 cm^{-1},[33,49] indicating that this carboxylate group is always protonated at pH 6.5 but deprotonated at pH 8.0 on reduction of Fe^{3+} to Fe^{2+} in Mn-depleted PSII. These observations imply that the pK_a of this group in the Fe^{2+} state is upshifted (from pK_a < 6.5 to 6.5 < pK_a < 8.5) on Mn depletion. Also, the changes in the spectral features at 1710–1700 cm^{-1} (Figure 5B) in the COOH region suggest the possibility that more than one carboxylate group is involved in protonation/deprotonation reactions affected by Mn depletion.

The structural perturbation of the Q_B site on Mn depletion was also demonstrated by the measurements of the Fe^{2+}/Fe^{3+} difference spectra in the presence of bromoxynil (Figure 6). The C≡N band of bromoxynil bound to the Q_B site was slightly upshifted from 2204 to 2206 cm^{-1} in the Fe^{2+} state on Mn depletion (Figure 6A). Previous docking calculations[33] predicted that the nitrogen of the C≡N group forms hydrogen bonds with the backbone NH of D1-Phe265 and the OH group of D1-Ser264, which exist on the opposite side of D1-His215 in the Q_B pocket. The upshift of the C≡N band indicates that the hydrogen bonds at the C≡N group are weakened and hence lengthened by Mn depletion. Therefore, it is suggested that Mn depletion slightly shifts the position of a polypeptide main chain, on which D1-Phe265 and D1-Ser264 are located, to a direction opposite that of the non-heme iron. The C=O of PQ in the Q_B site has also been suggested to interact with these two residues based on theoretical calculations[33,68] as well as the X-ray structure[31] (Figure 1). The weakened hydrogen bond between Q_B and these residues would shift the PQ to the D1-H215 side and strengthen the hydrogen bond between the other C=O of Q_B and D1-His215. This strengthened hydrogen bond is consistent with the pK_a upshift of D1-His215 observed in the 1093 cm^{-1} peak (Figure 5C).

The above FTIR data showed that Mn depletion affects the hydrogen-bond structure and the pK_a values of some protonatable amino acid residues around the non-heme iron and the Q_B site. These changes could be induced by the long-range interaction between the Mn_4CaO_5 cluster on the electron-donor side and the non-heme iron and Q_B sites on the electron-acceptor side via the transmembrane α-helices of the D1 subunit. The Mn_4CaO_5 cluster is formed mostly by interactions with the D1 subunit through the amino acid ligands on the C-terminal region (D1-Glu333, Asp342, and Ala344) connected to helix E and on the region between helices C and D (D1-Asp170 and Glu189), whereas D1-H215, Glu244, Ser264, and Phe265, which interact with the non-heme iron or Q_B and are affected by Mn depletion, are located on helix D or the D–E loop. Thus, it is most likely that the structural changes induced by the destruction of the Mn_4CaO_5 cluster is transferred to the above residues on the electron-acceptor side via transmembrane helices D and E.

The deprotonated anion form of the His ligand, most probably D1-His215, which was detected in the oxidized Fe^{3+} state in intact PSII (Figure 5C), should significantly decrease the $E_m(Fe^{2+}/Fe^{3+})$ value due to stabilization of the Fe^{3+} state. This, in turn, indicates that protonation of this residue by the pK_a increase on Mn depletion should upshift $E_m(Fe^{2+}/Fe^{3+})$. In contrast, the pK_a increase of a nearby Glu residue, which provided a negative 1750 cm^{-1} band (Figure 5B), in the Fe^{2+} state should downshift $E_m(Fe^{2+}/Fe^{3+})$. Thus, the relatively small upshift of +18 mV in $E_m(Fe^{2+}/Fe^{3+})$ by Mn depletion (Figure 3) can be interpreted as the consequence of the combination of these pK_a changes of His and Glu side chains, probably involving the effects of the COOH groups that show contributions at 1710–1700 cm^{-1} and other minor effects that were not detected in the present FTIR spectra.

The E_m shift of Q_A on Mn depletion has been reported to be ~+150 mV,[6−12] which is ~8 times greater than the E_m shift of the non-heme iron (+18 mV) observed in the present study. Previously, the $E_m(Q_A^-/Q_A)$ shift by −45 mV on binding of bromoxynil to the Q_B site was attributed to the effect of strong hydrogen bonding between the phenolate CO of bromoxynil and D1-His215 on the hydrogen-bond strength between Q_A and D2-His214 through the His-Fe-His bridge by FTIR measurements and theoretical calculations.[32,33,69] A similar effect of the transfer of the structural perturbation of the Fe-Q_B site to Q_A through the His-Fe-His bridge is expected to contribute to the change in $E_m(Q_A^-/Q_A)$ on Mn depletion. The upshift in the pK_a of D1-His215, indicative of a strengthened hydrogen bond, by Mn depletion (Figure 5C) may downshift

the $E_m(Q_A^-/Q_A)$ value, which is, however, an effect opposite of the reported positive $E_m(Q_A^-/Q_A)$ shift. In contrast, protonation of a Glu residue near the non-heme iron (likely D1-Glu244) in the Fe^{2+} state by the pK_a increase on Mn depletion (Figure 5B) should upshift the $E_m(Q_A^-/Q_A)$ value. These opposite effects, together with the effects by some other carboxylic groups (see above), may contribute to the reported shift of $E_m(Q_A^-/Q_A)$ by Mn depletion. Although detailed theoretical calculations are necessary to quantify the contributions of individual structural changes to the Q_A potential, it is presumed that the sum of these effects are not enough to explain the large $E_m(Q_A^-/Q_A)$ shift of +150 mV, which is based on the findings of this study demonstrating that the effect on $E_m(Fe^{2+}/Fe^{3+})$ was relatively small (+18 mV). Therefore, there could be other long-range interaction pathways to affect $E_m(Q_A^-/Q_A)$ more directly than the pathways via the D1 subunit around the non-heme iron and Q_B. This view is consistent with the previous observation that the effect of herbicide binding and that of Ca^{2+} binding on $E_m(Q_A^-/Q_A)$ are additive.[22]

Ishikita and Knapp[68] previously proposed that D2-Thr217 provides an additional hydrogen bond to Q_A on its reduction to induce the upshift of $E_m(Q_A^-/Q_A)$. However, FTIR measurements of Q_A^-/Q_A difference spectra in intact (in the form of $S_2Q_A^-/S_1Q_A$) and Mn-depleted PSII samples did not show any change in the frequency of the major CO peak of Q_A^-;[32] thus, a drastic change in the hydrogen-bond interaction, such as additional hydrogen bonding, does not seem to take place in the Q_A^- state. Recent DFT calculations of various hydrogen-bond models of PQ showed that although the effect of hydrogen bonding on the semiquinone CO frequency is relatively small (within 5 cm^{-1}), the change in the hydrogen-bond structure is reflected in the side bands around the main peak due to complex couplings with other vibrations of PQ and nearby amino acids.[70] It was also shown that the CO frequencies are affected by hydrogen-bond interactions more drastically in neutral PQ than in anionic PQ.[70] Thus, more detailed analysis of the Q_A^-/Q_A FTIR spectra, including the accurate assignment of the CO stretching vibrations of neutral Q_A in the 1700−1600 cm^{-1} region superimposing the amide I vibrations, in both intact and Mn-depleted PSII samples will be necessary to clarify the mechanism of the $E_m(Q_A^-/Q_A)$ change by Mn depletion.

■ ASSOCIATED CONTENT

Supporting Information

S_2Fe^{2+}/S_1Fe^{3+} and Fe^{2+}/Fe^{3+} difference spectra of the intact and Mn-depleted PSII membranes; S_2Fe^{2+}/S_1Fe^{3+}, S_2/S_1, and Fe^{2+}/Fe^{3+} difference spectra of the intact PSII membranes; and Fe^{2+}/Fe^{3+} difference spectra of Mn-depleted PSII membranes. This material is available free of charge via the Internet at http://pubs.acs.org.

■ AUTHOR INFORMATION

Corresponding Authors

*(Y.K.) E-mail: yuki.kato@bio.phys.nagoya-u.ac.jp. Telephone: +81-52-789-2881. Fax: +81-52-789-2883.

*(T.N.) E-mail: tnoguchi@bio.phys.nagoya-u.ac.jp.

Funding

This study was supported in part by the Grants-in-Aid for Scientific Research from the Japan Society for the Promotion of Science (JSPS) (25410009 to Y.K.; 24000018, 24107003, and 25291033 to T.N.) and by a Grant for Basic Science Research Projects from The Sumitomo Foundation (to Y.K.).

Notes

The authors declare no competing financial interest.

■ ABBREVIATIONS USED

Chl, chlorophyll; DCMU, 3-(3,4-dichlorophyenyl)-1,1-dimethylurea; E_m, redox potential; FTIR, Fourier transform infrared; MES, 2-(*N*-morpholino)ethanesulfonic acid; OTTLE, optically transparent thin-layer electrode; P680, the primary electron donor; Phe *a*, pheophytin *a*; PQ, plastoquinone; PSII, photosystem II; Q_A, primary quinone electron acceptor; Q_B, secondary quinone electron acceptor; SHE, standard hydrogen electrode

■ REFERENCES

(1) McEvoy, J. P., and Brudvig, G. W. (2006) Water-splitting chemistry of photosystem II. *Chem. Rev. 106*, 4455−4483.

(2) Messinger, J., Noguchi, T., and Yano, J. (2011) Photosynthetic O_2 evolution, in *Molecular Solar Fuels* (Wydrzynski, T., and Hillier, W., Eds.) pp 163−207, Chapter 7, Royal Society of Chemistry, Cambridge, UK.

(3) Cardona, T., Sedoud, A., Cox, N., and Rutherford, A. W. (2012) Charge separation in photosystem II: a comparative and evolutional overview. *Biochim. Biophys. Acta 1817*, 26−43.

(4) Renger, G. (2012) Photosynthetic water splitting: apparatus and mechanism, in *Photosynthesis: Plastid Biology, Energy Conversion and Carbon Assimilation* (Eaton-Rye, J. J., Tripathy, B. C., and Sharkey, T. D., Eds.) pp 359−414, Springer, Dordrecht, The Netherlands.

(5) Joliot, P. (2003) Period-four oscillations of the flash-induced oxygen formation in photosynthesis. *Photosynth. Res. 76*, 65−72.

(6) Krieger, A., and Weis, E. (1992) Energy-dependent of chlorophyll-*a*-fluorescence: the involvement of proton-calcium exchange at photosystem 2. *Photosynthetica 27*, 89−98.

(7) Krieger, A., Rutherford, A. W., and Johnson, G. N. (1995) On the determination of redox midpoint potential of the primary quinone electron acceptor, Q_A, in photosystem II. *Biochim. Biophys. Acta 1229*, 193−201.

(8) Johnson, G. N., Rutherford, A. W., and Krieger, A. (1995) A change in the midpoint potential of the quinone Q_A in photosystem II associated with photoactivation of oxygen evolution. *Biochim. Biophys. Acta 1229*, 202−207.

(9) Shibamoto, T., Kato, Y., Sugiura, M., and Watanabe, T. (2009) Redox potential of the primary plastoquinone electron acceptor Q_A in photosystem II from *Thermosynechococcus elongatus* determined by spectroelectrochemistry. *Biochemistry 48*, 10682−10684.

(10) Shibamoto, T., Kato, Y., Nagao, R., Yamazaki, T., Tomo, T., and Watanabe, T. (2010) Species-dependence of the redox potential of the primary quinone electron acceptor Q_A in photosystem II verified by spectroelectrochemistry. *FEBS Lett. 584*, 1526−1530.

(11) Ido, K., Gross, C. M., Guerrero, F., Sedoud, A., Lai, T.-L., Ifuku, K., Rutherford, A. W., and Krieger-Liszkay, A. (2011) High and low potential forms of the Q_A quinone electron acceptor in photosystem II of *Thermosynechococcus elongatus* and spinach. *J. Photochem. Photobiol., B 104*, 154−157.

(12) Allakhverdiev, S. I., Tsuchiya, T., Watabe, K., Kojima, A., Los, D. A., Tomo, T., Klimov, V. V., Mimuro, M., Redox potentials of primary electron acceptor quinone molecule $(Q_A)^-$ and conserved energetics of photosystem II in cyanobacteria with chlorophyll *a* and chlorophyll *d*, *Proc. Natl. Acad. Sci. U.S.A. 108*, 8054−8058.

(13) Diner, B. A. (1977) Dependence of the deactivation reactions of photosystem II on the redox state of plastoquinone pool a varied under anaerobic conditions: equillibria on the acceptor side of photosystem II. *Biochem. Biophys. Acta 460*, 247−258.

(14) Crofts, A. R., and Wraight, C. A. (1983) The electrochemical domain of photosynthesis. *Biochim. Biophys. Acta 726*, 149−185.

(15) Minagawa, J., Narusaka, Y., Inoue, Y., and Satoh, K. (1999) Electron transfer between Q_A and Q_B in photosystem II is thermodynamically perturbed in phototorelant mutants of *Synechocystis* sp. PCC 6803. *Biochemistry 38*, 770−775.
(16) Andréasson, L.-E., Vass, I., and Styring, S. (1995) Ca^{2+} depletion modifies the electron transfer on both donor and acceptor sides in Photosystem II from spinach. *Biochim. Biophys. Acta 1230*, 155−164.
(17) Hwang, H. H., and Burnap, R. L. (2005) Multiflash experiments reveal a new kinetic phase of photosystem II manganese cluster assembly in *Synechocystis* sp. PCC6803 *in vivo*. *Biochemistry 44*, 9766−9774.
(18) Krieger-Liszkay, A., Fufezan, C., and Trebst, A. (2008) Singlet oxygen production in photosystem II and related protection mechanism. *Photosynth. Res. 98*, 551−564.
(19) Vass, I. (2011) Role of charge recombination processes in photodamage and photoprotection of the photosystem II complex. *Physiol. Plant. 142*, 6−16.
(20) Kato, Y., Shitamobo, T., Yamamoto, S., Watanabe, T., Ishida, N., Sugiura, M., Rappaprot, F., and Boussac, A. (2012) Influence of the PsbA1/PsbA3, Ca^{2+}/Sr^{2+} and Cl^-/Br^- exchanges on the redox potential of the primary quinone Q_A in photosystem II from *Thermosynechococcus elongatus* as revealed by spectroelectrochemistry. *Biochim. Biophys. Acta 1817*, 1998−2004.
(21) Kargul, J., Maghlaoui, K., Murray, J. W., Deak, Z., Boussac, A., Rutherford, A. W., Vass, I., and Barber, J. (2007) Purification, crystallization and X-ray diffraction analyses of the *T. elongatus* PSII core dimer with strontium replacing calcium in the oxygen-evolving complex. *Biochim. Biophys. Acta 1767*, 404−413.
(22) Krieger-Liszkay, A., and Rutherford, A. W. (1998) Influence of herbicide binding on the redox potential of the quinone acceptor in photosystem II: relevance on photodamage and phytotoxicity. *Biochemistry 37*, 17339−17344.
(23) Rutherford, A. W., and Krieger-Liszkay, A. (2001) Herbicide-induced oxidative stress in photosystem II. *Trends Biochem. Sci. 26*, 648−653.
(24) Fufezan, C., Rutherford, A. W., and Krieger-Liszkay, A. (2002) Singlet oxygen production in herbicide-treated photosystem II. *FEBS Lett. 532*, 407−410.
(25) Petrouleas, V., and Crofts, A. R. (2005) The quinone iron acceptor complex, in *Photosystem II: The Light-Driven Water:-Plastoquinone Oxidoreductase* (Wydrzynski, T., and Satoh, K., Eds.) pp 177−206, Springer, Dordrecht, The Netherlands.
(26) Diner, B. A., Petrouleas, V., and Wendoloski, J. J. (1991) The ironquinone electron-acceptor complex of photosystem II. *Physiol. Plant. 81*, 423−436.
(27) Petrouleas, V., and Diner, B. A. (1986) Identification of Q_{400}, a high-potential electron acceptor of photosystem II, with the iron of the quinone-iron acceptor complex. *Biochim. Biophys. Acta 849*, 264−275.
(28) Zouni, A., Witt, H.-T., Kern, J., Fromme, P., Krauss, N., Saenger, W., and Orth, P. (2001) Crystal structure of photosystem II from *Synechococcus elongatus* at 3.8 Å resolution. *Nature 409*, 739−743.
(29) Ferreira, K. N., Iverson, T. M., Maghlaoui, K., Barber, J., and Iwata, S. (2004) Architecture of the photosynthetic oxygen-evolving center. *Science 303*, 1831−1838.
(30) Guskov, A., Kern, J., Gabdulkhakov, A., Broser, M., Zouni, A., and Saenger, W. (2009) Cyanobacterial photosystem II at 2.9-Å resolution and the role of quinones, lipids, channels and chloride. *Nat. Struct. Mol. Biol. 16*, 334−342.
(31) Umena, Y., Kawakami, K., Shen, J.-R., and Kamiya, N. (2011) Crystal structure of oxygen-evolving photosystem II at a resolution of 1.9 Å. *Nature 473*, 55−60.
(32) Takano, A., Takahashi, R., Suzuki, H., and Noguchi, T. (2008) Herbicide effect on the hydrogen-bonding interaction of the primary quinone electron acceptor Q_A in photosystem II as studied by Fourier transform infrared spectroscopy. *Photosynth. Res. 98*, 159−167.
(33) Takahashi, R., Hasegawa, K., Takano, A., and Noguchi, T. (2010) Structures and binding sites of phenolic herbicides in the Q_B pocket of photosystem II. *Biochemistry 49*, 5445−5454.
(34) Boussac, A., Sugiura, M., Lai, T.-L., and Rutherford, A. W. (2008) Low-temperature photochemistry in photosystem II from *Thermosynechococcus elongatus* induced by visible and near-infrared light. *Philos. Trans. R. Soc., B 363*, 1203−1210.
(35) Shibamoto, T., Kato, Y., and Watanabe, T. (2008) Spectroelectrochemistry of cytochrome b_{559} in the D1-D2-Cyt b_{559} complex from spinach. *FEBS Lett. 582*, 1490−1494.
(36) Kato, Y., Sugiura, M., Oda, A., and Watanabe, T. (2009) Spectroelectrochemical determination of the redox potential of pheophytin *a*, the primary electron acceptor in photosystem II. *Proc. Natl. Acad. Sci. U.S.A. 106*, 17365−17370.
(37) Sugiura, M., Kato, Y., Takahashi, R., Suzuki, H., Watanabe, T., Noguchi, T., Rappaport, F., and Boussac, A. (2010) Energetics in photosystem II from *Thermosynechococcus elongatus* with a D1 protein encoded by either the $psbA_1$ or $psbA_3$ gene. *Biochim. Biophys. Acta 1797*, 1491−1499.
(38) Noguchi, T., and Berthomieu, C. (2005) Molecular analysis by vibrational spectroscopy, in *Photosystem II: The Light-Driven Water:-Plastoquinone Oxidoreductase* (Wydrzynski, T., and Satoh, K., Eds.) pp 367−387, Springer, Dordrecht, The Netherlands.
(39) Debus, R. J. (2008) Protein ligation of the photosynthetic oxygen-evolving center. *Coord. Chem. Rev. 252*, 244−258.
(40) Noguchi, T. (2008) Fourier transform infrared analysis of the photosynthetic oxygen-evolving center. *Coord. Chem. Rev. 252*, 336−346.
(41) Berthomieu, C., and Hienerwadel, R. (2009) Fourier transform infrared (FTIR) spectroscopy. *Photosynth. Res. 101*, 157−170.
(42) Noguchi, T. (2013) Monitoring the reactions of photosynthetic water oxidation using infrared spectroscopy. *Biomed. Spectrosc. Imaging 2*, 115−128.
(43) Chu, H.-A. (2013) Fourier transform infrared difference spectroscopy for studying the molecular mechanism of photosynthetic water oxidation. *Frontiers Plant Sci. 4*, No. 146.
(44) Ikegami, I., and Katoh, S. (1973) Studies on chlorophyll fluorescence in chloroplasts II. Effect of ferricyanide on the induction of fluorescence in the presence of 3-(3,4-dichlorophynyl)-1,1-dimethylurea. *Plant Cell Phys. 14*, 829−836.
(45) Bowes, J., Crofts, A. R., and Itoh, S. (1979) A high potential acceptor for photosystem II. *Biochim. Biophys. Acta 547*, 320−335.
(46) Renger, G., Wacker, U., and Völker, M. (1987) Studies on the protolytic reactions coupled with water cleavage in photosystem II membrane fragments from spinach. *Photosynth. Res. 13*, 167−189.
(47) Deligiannkis, Y., Petrouleas, V., and Diner, B. A. (1994) Binding of carboxylate anions at the non-heme Fe(II) of PSII. I Effects on the $Q_A^-Fe^{2+}$ and Q_AFe^{3+} EPR spectra and the redox properties of the iron. *Biochim. Biophys. Acta 1188*, 260−270.
(48) Noguchi, T., and Inoue, Y. (1995) Identification of Fourier transform infrared signals from the non-heme iron in photosystem II. *J. Biochem. 118*, 9−12.
(49) Hienerwadel, R., and Berthomieu, C. (1995) Bicarbonate binding to the non-heme iron of photosystem II investigated by Fourier transform infrared difference spectroscopy and ^{13}C-labeled bicarbonate. *Biochemistry 34*, 16288−16297.
(50) Berthomieu, C., and Hienerwadel, R. (2001) Iron coordination in photosystem II: interaction between bicarbonate and the Q_B pocket studied by Fourier transform infrared spectroscopy. *Biochemistry 40*, 4044−4052.
(51) Aoyama, C., Suzuki, H., Sugiura, M., and Noguchi, T. (2008) Flash-induced FTIR difference spectroscopy shows no evidence for structural coupling of bicarbonate to the oxygen-evolving Mn cluster in photosystem II. *Biochemistry 47*, 2760−2765.
(52) Takahashi, R., Boussac, A., Sugiura, M., and Noguchi, T. (2009) Structural coupling of a tyrosine side chain with the non-heme iron center in photosystem II as revealed by light-induced Fourier transform infrared difference spectroscopy. *Biochemistry 48*, 8994−9001.
(53) Ono, T., and Inoue, Y. (1986) Effects of removal and reconstitution of the extrinsic 33, 24 and 16 kDa proteins on flash

oxygen yield in photosystem II particles. *Biochim. Biophys. Acta 850*, 380−389.
(54) Noguchi, T., Ono, T., and Inoue, Y. (1995) Direct detection of a carboxylate bridge between Mn and Ca^{2+} in the photosynthetic oxygen-evolving center by means of Fourier transform infrared spectroscopy. *Biochim. Biophys. Acta 1228*, 189−200.
(55) Moss, D., Nabedryk, E., Breton, J., and Mäntele, W. (1990) Redox-linked confromational changes in proteins detected by a combination of infrared spectroscopy and protein electrochemitsry. *Eur. J. Biochem. 187*, 565−572.
(56) Best, S. P., Borg, S. J., and Vincent, K. A. (2008) Infrared spectroelectrochemistry, in *Spectroelectrohcemistry* (Klaim, W., and Klein, A., Eds.) pp 1−30, Royal Society of Chemistry, Cambridge, UK.
(57) Taniguchi, I., Toyosawa, K., Yamaguchi, H., and Yasukouchi, K. (1982) Voltammetric response of horse heat cytochrome *c* at a gold electrode in the presence of sulfur bridged bipyridines. *J. Electroanal. Chem. 140*, 187−193.
(58) Noguchi, T., and Sugiura, M. (2003) Analysis of flash-induced FTIR difference spectra of the S-state cycle in the photosynthetic water-oxidizing complex by uniform ^{15}N and ^{13}C isotope labeling. *Biochemistry 42*, 6035−6042.
(59) Kimura, Y., Mizusawa, N., Ishii, A., Yamanari, T., and Ono, T. (2003) Changes of low-frequency vibrational modes induced by universal ^{15}N- and ^{13}C-isotope labeling in S_2/S_1 FTIR difference spectrum of oxygen-evolving complex. *Biochemistry 42*, 13170−13177.
(60) Nie, B., Stutzman, J., and Xie, A. (2005) A vibrational spectral marker for probing the hydrogen-bonding status of protonated Asp and Glu residues. *Biophys. J. 88*, 2833−2847.
(61) Takei, K.-I., Takahashi, R., and Noguchi, T. (2008) Correlation between the hydrogen-bond structures and the C═O stretching frequencies of carboxylic acids as studied by density functional theory calculations: theoretical basis for interpretation of infrared bands of carboxylic groups in proteins. *J. Phys. Chem. B 112*, 6725−6731.
(62) Lutz, M., and Mäntele, W. (1991) Vibrational spectroscopy of chlorophylls, in *Chlorophylls* (Scheer, H., Ed.) pp 855−902, CRC Press, Boca Roton, FL.
(63) Müh, F., and Zouni, A. (2013) The nonheme iron in photosystem II. *Photosynth. Res. 116*, 295−314.
(64) Mamedov, M. D., Tyunyakina, A. A., Siletsyky, S. A., and Semenov, A. Y. (2006) Voltage changes involving photosystem II quinone-iron complex turnover. *Eur. Biophys. J. 35*, 647−654.
(65) McEvoy, J. P., and Brudvig, G. W. (2008) Redox reactions of the non-heme iron in photosystem II: an EPR spectroscopic study. *Biochemistry 47*, 13394−13403.
(66) Hasegawa, K., Ono, T., and Noguchi, T. (2000) Vibrational spectra and *ab initio* DFT calculations of 4-methylimidazole and its different protonation forms: infrared and Raman markers of the protonation state of a histidine side chain. *J. Phys. Chem. B 104*, 4253−4265.
(67) Ishikita, H., and Knapp, E. W. (2005) Oxidation of the non-heme iron complex in photosystem II. *Biochemistry 44*, 14772−14783.
(68) Ishikita, H., and Knapp, E. W. (2005) Control of quinone redox potentials in photosystem II: electron transfer and photoprotection. *J. Am. Chem. Soc. 127*, 14714−14720.
(69) Ishikita, H., Hasegawa, K., and Noguchi, T. (2011) How does the Q_B site influence propagate to the Q_A site in photosystem II. *Biochemistry 50*, 5436−5442.
(70) Ashizawa, R., and Noguchi, T. (2014) Effects of hydrogen bonding interactions on the redox potential and molecular vibrations of plastoquinone as studied by density functional theory calculations. *Phys. Chem. Chem. Phys. 16*, 11864−11876.